Effects of small ionic amphiphilic additives on reverse microemulsion morphology

Research Highlights

- Cylindrical morphologies of reverse microemulsions induced by small molecule hydrotropes.
- Ellipsoidal droplets of high aspect ratio in reverse AOT microemulsions are induced by short chain alkanoate additives.
- A cylinder to sphere transition in reverse AOT microemulsions is seen with increasing water content.

Effects of small ionic amphiphilic additives on reverse microemulsion morphology

Marios Hopkins Hatzopoulos[1]

Craig James[1]

Sarah Rogers[2]

Isabelle Grillo[3]

Peter J. Dowding[4]

Julian Eastoe[*1]

1 School of Chemistry, University of Bristol, Cantock's Close, Bristol, BS8 1TS, UK

2 ISIS-STFC, Rutherford Appleton Laboratory, Chilton, Oxon OX11 0QX, United Kingdom

3. ILL, BP 156-X, F-38042 Grenoble Cedex, France

4. Infineum UK Ltd., Milton Hill Business & Technology Centre, Abingdon, Oxfordshire OX13 6BB, UK

* Corresponding author

Corresponding author contact details:

Prof. Julian Eastoe

julian.eastoe@bristol.ac.uk

tel +44 (0)117 92 89180

fax +44 (0)117 92 77985

Abstract

Hypothesis

Initial studies [Journal of Colloid and Interface Science 392 (2013) 304–310] have shown that ionic hydrotropic additives can drive a sphere–to-cylinder (ellipsoid) transition in water-in-oil (w/o) microemulsions stabilized by the anionic surfactant Aerosol-OT; however the origins of this behaviour remained unclear. Here systematic effects of chemical structure are explored with a new set of hydrotropes, in terms of an aromatic versus a saturated cyclic hydrophobic group, and linear chain length of alkyl carboxylates. It is proposed that hydrotrope-induced microemulsion sphere-to-cylinder (ellipsoid) transitions are linked to additive hydrophobicity, and so a correlation between the bulk aqueous phase critical aggregation concentration (*cac*) and perturbation of microemulsion structure is expected.

Experiments

Water-in-oil microemulsions were formulated as a function of water content *w* (= [water]/[AOT]) and concentration of different hydrotropes, being either cyclic (sodium benzoate or sodium cyclohexanoate), or linear chain systems (sodium hexanoate, sodium heptanoate and sodium octanoate). Phase behaviour studies were performed as a function of *w,* additive type and temperature at total surfactant concentration [S_T] = 0.10 M and constant mole fraction *x* = 0.10 (*x* = [hydrotrope]/[S_T]). Microemulsion domain structures were investigated by small-angle neutron scattering (SANS), and these data were fitted by structural models to yield information on the shapes (spheres, ellipsoids or cylinders) and sizes of the nanodroplets.

Findings

Under the conditions of study hydrotrope chemical structure has a significant effect on microemulsion structure: sodium cyclohexanoate does not induce the formation of cylindrical/ellipsoidal nanodroplets, whereas the aromatic analogue sodium benzoate does. Furthermore, the short chain sodium hexanoate does not cause anisotropic microemulsions, but the more hydrophobic longer chain heptanoate and octanoate analogues do induce sphere-to-ellipsoid transitions. This study shows that underlying microemulsion structures can be tuned by hydrotropes, and that the strength of the effect can be identified with hydrotrope hydrophobicity in terms of the bulk aqueous phase *cac*.

Keywords: microemulsions; hydrotropes; nanostructures; phase behavior; small-angle neutron scattering

Introduction

Microemulsions are systems of significant interest in both academic studies and for industrial applications. Microemulsions comprise two or more immiscible or partially miscible fluids, stabilised by added surfactants. The surfactants must reduce interfacial tensions sufficiently for nanometre scale domains to form, which gives microemulsions their characteristic transparency (translucency), visually distinguishing them to other types of emulsions. The visual appearance of microemulsions does not change with time, inferring thermodynamic stability, a further distinguishing feature to other emulsions. These properties and features lead to applications of microemulsions as nanoreactors in chemical [1] and nanoparticle synthesis [2], as nanoparticle recovery vehicles [4], in soil remediation processes, enhanced oil recovery [5], pharmaceutical delivery [6], and engine oil and fuel additives [7].

With such an array of applications, control over microemulsion properties becomes important. The phase behaviour with respect to composition, pressure and temperature are the most common property levers. The size of the microemulsion nanodomains can be varied by increasing the amounts of dispersed phase added. Size control in reverse microemulsions, for example, at constant water content can be attained by the choice of surfactant and (or) cosurfactant chemical structure.

Microemulsions are more than often reported as spherical [2-4]. Axial elongation of microemulsions or reverse hydrated micelles (in the cases of low water content reverse phases) in oil media and supercritical CO_2 is of interest for control over viscosity. To this end surfactant systems exhibiting axially elongated aggregation structures have been the topic of on-going research [8, 9]. Such structures, commonly encountered in aqueous phases, are catanionic systems where the long chain ion is a cation and the ‘counter ion’ is a small molecule amphiphilic additive, commonly called a hydrotrope [8]. An example hydrotrope is sodium benzoate, which may be considered as a “primitive” short chain surfactant. The presence of a bulky hydrotrope is recognised as being critical for micellar elongation, with these systems shown to produce substantial increases in solution viscosities [10]. Close investigation by NMR and computer simulations revealed that the hydrotrope counterions adsorb at the micellar interfacial region [11]. In mixed solutions of surfactants and hydrotropes of the same charge only ellipsoidal structures have

been observed [12]. The difference between the two systems is likely being the difference in the interfacially adsorbed amount of hydrotrope. In catanionic systems the two ions cannot separate or partition due to electrostatic attraction. In systems of mixed surfactants and hydrotropes of the same charge the electrostatic repulsion diminishes interfacial co-adsorption.

Elongated microemulsions were discovered by Petit [13] and Eastoe *et al.* [14-16] who first observed cylindrical or ellipsoidal reverse microemulsions with the Aerosol-OT (AOT) anion coupled with Cobalt counterions (substituted for the normally found Sodium ion). This work was taken further to explore the effects of different metal counterions on AOT microemulsion morphology [14-16], and recently showing elongated self-assembly structures in supercritical CO_2 with related surfactants [17].

More recently, mixed AOT microemulsions containing anionic hydrotropes in the aqueous phase have been shown to stabilize cylindrical nanostructures that change to spherical micelles with increasing microemulsion water content (w = [water]/[surf]) [18]. Three structurally related homologous series of alkyl-hydrotropes were examined as additives in reverse AOT microemulsions with heptane as oil [18]. The additives ranged in size from short to medium chain length ‘alkyl-hydrotropes’. The effect of axial elongation was attributed to two features of the additives, (i) the hydrophobicity and plausibly strength of adsorption of the molecules at the water/oil interface and (ii) the position of the ring moieties in the molecules. Because hydrotropes do not partition strongly into oil (they are only weakly hydrophobic), at low water content the effective hydrotrope concentration in the water pools is high, and hence they might be expected to adsorb strongly at the interface. For a fixed mole fraction x of hydrotrope in the total microemulsion, increasing the water content w decreases the additive concentration in the water droplets, and eventually the micellar geometry change to spherical, as found for the native AOT (hydrotrope-free) systems [19]. However, the extent of axial elongation did not appear to directly correlate to additive architecture, with some less hydrophobic additives inducing longer cylinders as compared to the more hydrophobic homologues and analogues.

Here an attempt is made to isolate the two parameters, chemical structure and hydrophobicity, by comparing the effects of subtle structural changes in the hydrotropes (aromatic sodium benzoate and saturated sodium cyclohexanoate, and

chain length with sodium hexanoate, heptanoate and octanoate) on the morphology of reverse AOT microemulsions.

Experimental

Materials

Sodium bis(2-ethylhexyl)sulfosuccinate (Aerosol-OT, AOT, 98%) was purchased from Aldrich. Purification of AOT was carried out by dissolving the surfactant in double distilled methanol. The solution was allowed to stand overnight, after which NaCl precipitated. The supernatant solution was removed and centrifuged at 600 rpm for 30 min to remove any suspended salt crystals. The solvent was then removed by rotary evaporation and the product was dried over phosphorous pentoxide in a vacuum over at 60 ^{o}C overnight. Sodium octanoate, sodium heptanoate, sodium hexanoate and sodium benzoate were purchased from Aldrich and used as received. Sodium cyclohexanoate was prepared from its parent acid (also purchased form Aldrich at the highest purity available) as described elsewhere [20]. Microemulsions were prepared at total surfactant concentration [S_T] = 0.10 M and x = 0.10 (x = [hydrotrope]/[S_T]), by mixing an appropriate AOT in *n*-heptane solution with a hydrotrope-D_2O solution (these solutions were not pH adjusted), adding D_2O and *n*-heptane to the required w values and total volume respectively and shaking until optically homogenous.

Phase behaviour

Temperature scans were carried out at 1 ^{o}C increments in a thermostated water bath with an error of 0.2 ^{o}C. The samples were allowed to thermally equilibrate for 20 min between temperature increments and examined visually.

SANS

Small-angle neutron scattering measurements were carried out on the LOQ instrument at ISIS at the Rutherford Appleton Laboratory with the exception of w = 5 AOT-Benzoate, w = 10 for AOT-hexanoate and w = 10 and w = 20 for AOT-heptanoate and AOT-octanoate microemulsions, which were measured on D11 instrument at the Institut Laue Langevin, Grenoble France. Samples were contained in 1 mm path-length Hellma cells and thermostated at 20$\pm$0.1 ^{o}C. On LOQ the detector distance was set at 1.2 m and 8 m with respective distances from the collimator at 4 m and 8 m. The incident wavelength λ = 10 Å, giving rise to a Q range

of ~0.005-0.3 Å^{-1}. On D11 the incident wavelength was λ = 10 Å with detector distances at 1.2 m and 8 m and respective collimator distances at 5.3 m and 8 m, giving rise to a Q range of ~0.003-0.3 Å^{-1}.
The momentum transfer Q is defined as:

$$Q = \frac{4\pi \sin(\theta/2)}{\lambda} \quad (1)$$

where θ is the scattering angle and λ is the incident neutron wavelength.

The data were fitted using the least squares FISH program [21]. For colloidal particles the scattering profile curve is broadly described by:

$$I(Q) \propto P(Q)S(Q) \quad (2)$$

where *P(Q)* is a form factor, which contains information about the size and shape of the aggregates, and *S(Q)* is a structure factor reporting on interactions. In this case of non-interacting particles *S(Q)* tends to unity. Trials with models various *P(Q)* functions were carried out with parameters related to *S(Q)* where absent. First approximation radii were derived by Guinier analysis and used as a starting point for model fitting. Scale factors (*SF*) were calculated using

$$SF = \Phi \Delta\rho^2 10^{-24} \quad (3)$$

where $\Delta\rho$ ($\rho_{D_2O} - \rho_{oil}$) is difference in scattering length densities of the D_2O core and oil (*n*-heptane in this case) and Φ is the volume fraction of the water core.

Residual backgrounds were estimated directly from the data by visual inspection. Once a first reasonable initial fit was obtained from the calculated inputs the remaining parameters were floated and minimized for more accurate fits.

Results and discussion

Phase behaviour

The behaviour of the AOT-hydrotrope and AOT-Alkanoate microemulsions with increasing water content *w* and temperature T is shown in Figure 1. Microemulsions containing octanoate and heptanoate exhibit a higher water solubilisation capacity than those containing hexanoate, benzoate and cyclohexanoate. In the case of AOT-alkanoates a shrinking lower-water content capacity and a broadening higher-water capacity accompanied by an overall shift to lower temperatures is observed. This behaviour appears to gradually change with increasing alkanoate tail length. The AOT microemulsions shift stability region with increasing alkanoate chain length to lower temperatures and closer to the temperature range of stability for normal (hydrotrope-free) AOT microemulsions [19]. The longer the tail length the greater the 'alkyl' character of the additive and a stronger positive interaction between the additive and AOT tails is expected.

In the case of hydrotrope additives a similar behaviour to previously reported AOT-alkyl-hydrotrope combinations is observed [18]. The saturated hydrotrope shifts the phase diagram to lower temperatures with respect to the aromatic benzoate, and hence again closer to the stability temperature region of pure AOT microemulsions; behaviour observed for the lower alkyl-hydrotrope analogues studied in [18]. This was attributed to the more favourable interactions between the saturated and hence more alkane-like nature of the cyclohexanoate hydrophobic moiety with the AOT alkyl tails, than the aromatic benzoate.

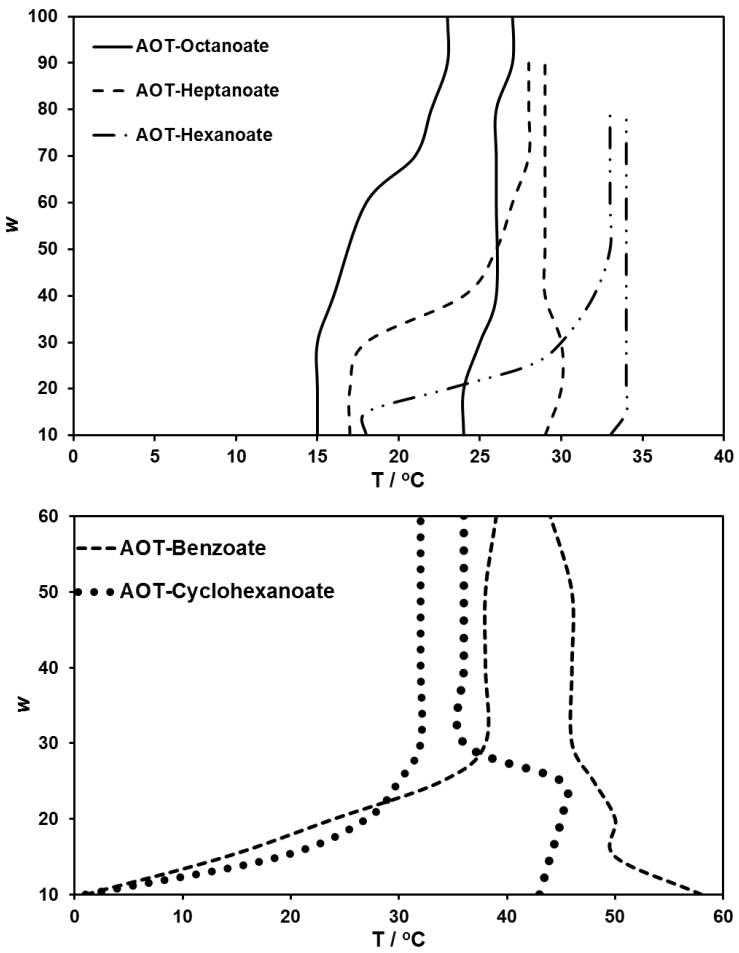

Figure 1. Phase behaviour of water-in-oil microemulsions containing AOT+linear chain alkanoates (top) and AOT+cyclic hydrotropes (bottom).

Small-angle Neutron Scattering

Reverse AOT/*n*-heptane/D_2O microemulsions are known to be spherical with radius increasing proportionally with water content *w* [19]. In a previous study alkyl-hydrotropes induced a varying degree of axial elongation with rods and ellipsoids observed at *w* values where the corresponding concentration of the additive was above or in close proximity of the corresponding bulk critical aggregation concentration (*cac* or critical micelle concentration *cmc*), and below which the microemulsions became spherical [18]. Here the effects of architecture and hydrophobicity are examined. In Table 1 the species and *cmc* values are reported. The *cac* (*cmc*) for sodium heptanoate and hexanoate are estimated by calculation, using the Klevens equation [20, 22] (equation 4) for the sodium alkanoate series, where the hydrophobic chain length *n* is related to the *cmc*.

$$\log(cmc) = -0.2832n + 1.5145 \qquad 4$$

Table 1. Critical micelle/aggregate concentrations of hydrotrope additives.

Additive	*cmc* / M	Ref.
Sodium benzoate	0.48	19
Sodium cyclohexanoate	0.97	23
Sodium hexanoate	1.25	Calculated
Sodium heptanoate	0.65	Calculated
Sodium octanoate	0.34	24

SANS profiles

In Figure 2 the scattering profile of the sodium benzoate containing system for *w* = 5 and 10 shows a power law decay in the intermediate-low Q range of approximately -1, indicative of an elongated structures. For the higher water content the gradient becomes 0, as is the case for the profile of sodium hexanoate in Figure 3, which corresponds to non-interacting spherical particles [19, 25]. For AOT-hexanoate

mixtures, shown in Figure 3, all profiles exhibit an essentially no power law. The cases of sodium octanoate (Figure 4) and heptanoate (Figure 3) are interesting as, like benzoate, they exhibit the power law decay which approaches -1 for *w* = 10 becomes 0 for higher water content values.

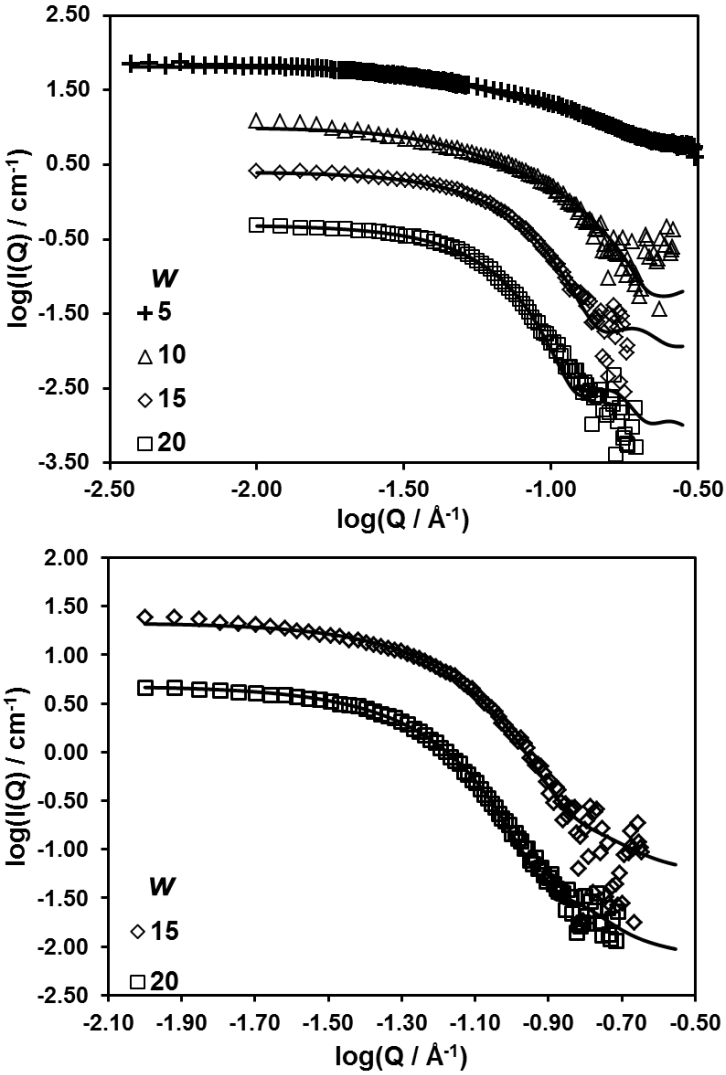

Figure 2 Scattering profiles from water-in-oil microemulsions with AOT-benzoate (top) (profiles shifted vertically: *w* = 5, *w* = 15 and *w* = 20 by +1.5, -1 and -2) and AOT-cyclohexanoate (bottom) microemulsions at various *w* values (profiles shifted vertically: *w* = 20 by -1).

Table 2 Parameters from analyses of SANS data of water-in-oil microemulsions with *w* denoting the water content, *y* the ratio of the effective concentration of additive in the droplet in relation to the bulk *cmc*/*cac*, *R* the radius, $\bar{R}$ the mean radius, *L* the rod length, *J* the ellipsoid aspect ratio, *σ* the polydispersity of spheres and R^G is the Guinier radius.

			Fitting parameters				Guinier radius
Additive	***w***	***y***	**model**	$\bar{R} \pm 1$ **/ Å**	***L* / Å**	***J***	R^G **/ Å**
Sodium benzoate	**5**	2.31	Rod	12.0	100.0	-	8.5
	10	1.16		16.6	99.7		18.8
	15	0.77	Ellipsoid	27.9		1.75	36.7
	w	***y***	**model**	$\bar{R} \pm 1$ **/ Å**		***σ***	R^G **/ Å**
	20	0.58	Schultz polydisperse spheres	34.1	-	0.22	45.2

			Fitting parameters			Guinier radius
Additive	***w***	***y***	**model**	$\bar{R} \pm 1$ **/ Å**	***σ***	R^G **/ Å**
Sodium cyclohexanoate	**15**	0.38	Schultz polydisperse spheres	27.1	0.21	36.0
	20	0.29		31.5	0.23	43.2

The slope of the linear region of $ln(I(Q)Q^D)$ plotted against Q^2 is proportional to the effective radius *R* by *R/2* for disks, *R/4* for cylinder and *R/5* for spheres [26]. Guinier analysis radii reported in the tables depend on the type model analysis. In other words for *w* values fitted with the Schultz polydisperse spheres model a Guinier sphere analysis was employed, and for *w* values fitted with the ellipsoid and rod models the reported radii are those of Guinier cylinder analysis. In some cases such as those of higher *w* values for AOT-benzoate and AOT-cyclohexanoate may be fitted by both Schultz polydisperse spheres and the ellipsoid model, with decision on the more appropriate fitting following the better fit in the higher *Q* region and the

plausibility of polydispersities. The tables also report the length of the rods *L*, aspect ratio *J* of ellipsoids and polydispersities σ of spheres. To make direct comparisons easier we introduce the parameter $y = [hydrotrope]_{aq} / cac$, where $[hydrotrope]_{aq}$ is the effective hydrotrope concentration in the aqueous phase, assuming no partitioning into the oil phase.

Table 2 reports the fitting parameters derived from least square model fitting of the profiles of sodium benzoate which produced axial elongation corresponding to a rod model at $w = 5$ and $w = 10$, at which concentrations the additive is above its bulk solution *cac* (*cmc*). It is interesting to observe that at $w = 5$ the radius is smaller than $w = 10$ (as expected); however the length of the cylinder is the same in both cases, however keeping in mind that this is an averaged picture and the model does not account for polydispersity. Ellipsoids were produced at $w = 15$ and spheres at $w = 20$ where the concentrations are still below but relatively close to the *cac* ($y = 0.77$ and 0.58 respectively), behaviour in line with the alky-benzoates reported in [18]. As mentioned above sodium cyclohexanoate can be fitted by both the Schultz polydisperse and ellipsoid model fairly well at $w = 15$. However in view of previous and the concentration at all *w* values being well below its previously determined *cac* [23], we report the parameters of polydisperse spheres and hence do not consider a case where these particles are ellipsoid.

Alkanoates have not been reported before to induce any change in aggregate morphology when employed as additives to aqueous solutions of other surfactants of same charge, in microemulsion systems, or as counterions in catanionic surfactants. Interestingly, here sodium heptanoate (Table 3) and sodium octanoate (Table 4) at $w = 10$ produce reasonably elongated ellipsoid structures. At $w = 10$ sodium octanoate and heptanoate are just above and just below their *cmc* values respectively with *y* values of 1.16 and 0.85 respectively. At $w = 20$ both additives are below their *cmc* values and the structures become spherical. Heptanoate at $y = 0.85$ ($w = 10$) produces ellipsoids however at the similar value of 0.82 ($w = 20$) octanoate forms spheres. Sodium hexanoate is below its *cmc* at all concentrations investigated and all profiles reported are fitted using the Schultz model for polydisperse spheres (Table 3), with good agreement.

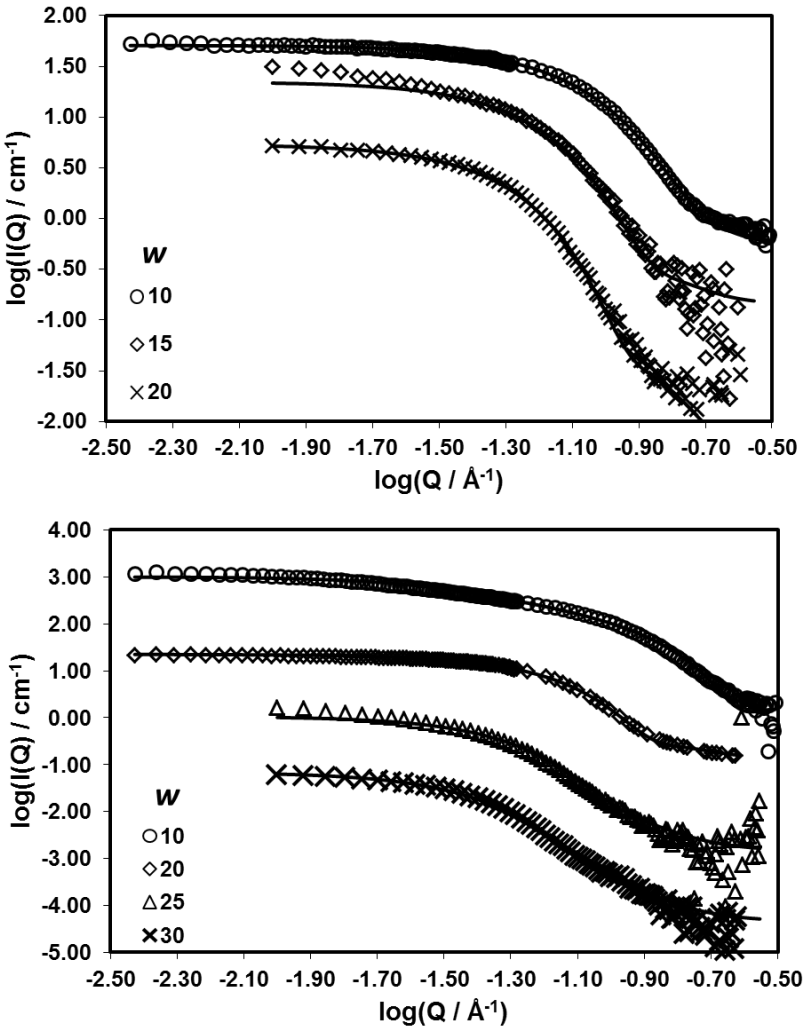

Figure 3 Scattering profiles from water-in-oil microemulsions with AOT-hexanoate (top) values (profiles shifted vertically: *w* = 10 by +1, *w* = 20 by -1) and AOT-heptanoate (bottom) (profiles shifted vertically: *w* = 10 by +2, *w* = 25 by -2 and *w* = 30 by -3.5) microemulsions at various *w.*

Table 3 Parameters from analyses of SANS data of water-in-oil microemulsions containing AOT–hexanoate, AOT-heptanoate, with *w* denoting the water content, *y* the ratio of the effective concentration of additive in the droplet in relation to the bulk *cmc*/*cac*, *R* the radius, $\bar{R}$ the mean radius, *J* the ellipsoid aspect ratio, *σ* the polydispersity of spheres and R^G is the Guinier radius.

			Fitting parameters			Guinier radius
Additive	***w***	***y***	**model**	$\bar{R} \pm 1$ **/ Å**	***σ***	R^G **/ Å**
Sodium Hexanoate	**10**	0.44	Schultz polydisperse spheres	21.0	0.20	25.7
	15	0.30		27.8	0.22	34.1
	20	0.22		32.6	0.26	44.8
			Fitting parameters			**Guinier radius**
Additive	***w***	***y***	**model**	$R \pm 1$ **/ Å**	***J***	R^G **/ Å**
Sodium Heptanoate	**10**	0.85	Ellipsoid	16.7	6.00	20.5
	w	***y***	**model**	$\bar{R} \pm 1$ **/ Å**	***σ***	R^G **/ Å**
	20	0.43	Schultz polydisperse spheres	29.3	0.20	34.8
	25	0.34		34.8	0.28	55.3
	30	0.28		39.2	0.33	60.7

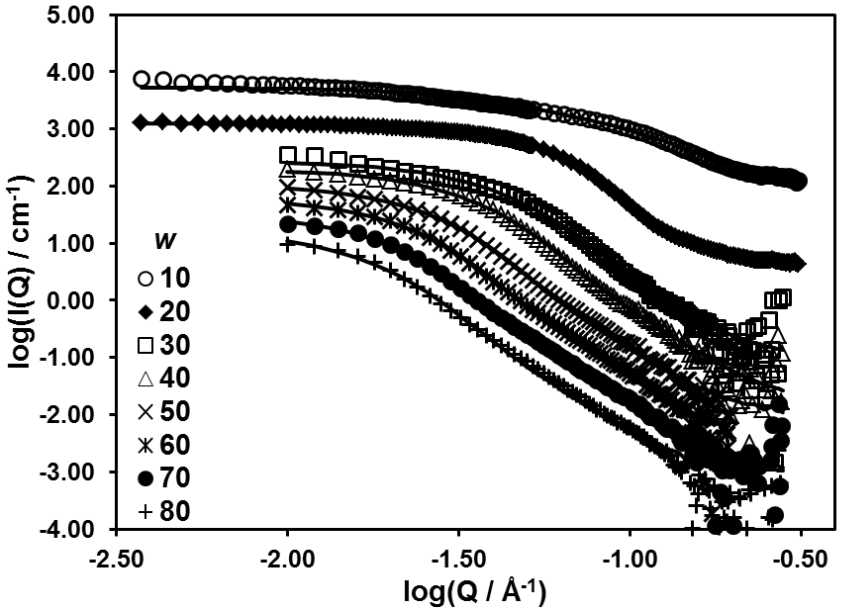

Figure 4 Scattering profiles of AOT-octanoate microemulsions at various *w* values (profiles shifted vertically: *w* = 10 by +3,*w* = 20 by +0.5, *w* = 40 by-0.5, *w* = 50 by -1, *w* = 60 by -1.5, *w* = 70 by -2 and *w* = 80 by -2.5).

Table 4. Parameters from analyses of SANS data of water-in-oil microemulsions containing AOT–octanoate hydrotrope with denoting *w* the water content, *y* is the ratio of the effective concentration of additive in the droplet in relation to the bulk *cmc*/*cac*, *R* is the radius, $\bar{R}$ is the mean radius, *J* is the ellipsoid aspect ratio, *σ* is the polydispersity of spheres and R^G is the Guinier radius.

		Fitting parameters			Guinier radius
w	***y***	**model**	$\bar{R} \pm 1$ **/ Å**	***J***	R^G **/ Å**
10	1.63	Ellipsoid	14.3	5.32	14.7
w	***y***	**model**	$\bar{R} \pm 1$ **/ Å**	***σ***	R^G **/ Å**
20	0.82	Schultz polydisperse spheres	31.6	0.22	41.7
30	0.54		37.3	0.31	51.1
40	0.41		45.2	0.32	69.7
50	0.33		55.1	0.36	86.6
60	0.27		64.7	0.35	105.8
70	0.23		71.5	0.37	121.5
80	0.20		75.7	0.40	133.1

The ellipsoidal droplets formed with sodium heptanoate have longer primary axes than those of octanoate. In the case of AOT-alkylbenzoate mixtures, sodium butylbenzoate produced stronger elongation than sodium octylbenzoate and both were more effective than sodium ethylbenzoate [18], which is interesting considering the phase behaviour of these mixtures, where the longer additives produce greater stability, and hence can be thought of as more compatible with the AOT chains.

At their largest *y* values of 0.44, 0.85, 1.63 the fitted radii of hexanoate, heptanoate and octanoate mixed AOT systems are 18.3 Å, 16.7 Å and 14.3 Å respectively. In other words the radii decrease with increasing additive chain length, whilst for $w = 20$ where the *y* values are 0.22, 0.43 and 0.82 the trend changes with the radii being 32.6 Å, 29.3 Å and 30.6 Å respectively. Pure AOT microemulsions have radii of 21.6 Å and 32.9 Å for $w = 10$ and $w = 20$ respectively [19]. The presence of the additives causes a noticeable decrease in the mean radii of the microemulsions for any *w* value, at the same time the polydispersity increases with water content. This phenomenon was also observed with alcohols adsorbing at the reverse microemulsion interface formed by the zwitterionic 1,2-*n*-octanoyl-*sn*-glycero-3-phosphocholine surfactant in hexane [27]. In the aforementioned systems pentanol, hexanol and octanol were studied by SANS contrast variation, with the alcohols being increasingly hexane-soluble with increasing alcohol chain length, and vice versa for water [27]. In reverse microemulsions of a dichain cationic surfactant, whose one branch was kept at constant length and the other varied, contrast variation-SANS revealed a greater degree of solvent penetration when the two chain had a greater difference in length. It was also noted that the solubilisation phase boundary w_{max} decreased with the radius and polydispersity at that boundary with surfactant asymmetry. Mixing increasing amounts of the single chain surfactant to its dichain analogue showed that at a constant w_{max} value the droplet radius increased and polydispersity decreased. It was argued that with the head group area being approximately constant the effective chain volume decreased and hence a more planar film was favoured, which in turn allows for greater water solubility. In a later study the same authors showed that at a constant *w* value increasing the amount of DTAB at the expense of DDAB caused an increase in both radius and polydispersity [28]. Furthermore, it was established that the two surfactants were ideally mixed, indicating that the ratio of the two surfactants at the interface was the same as that in

the bulk phase. The difference in the *cmc* values of the alkanoates to AOT is on the order of magnitude. Further still there are significant differences in hydrophobicity between the alkanoates themselves. Therefore it is plausible to suggest that the interfacial composition may not reflect the actual composition of the mixtures, though contrast variation experiments would be ideal for the assessment of this statement. Then direct comparisons of *w* profiles may be limited to the similarity in size. A way of addressing the difference in hydrophobicity of the additives is by comparing the microemulsion radii at the same *y* values. Figure 5 shows that larger water drops are stabilised by longer alkanoates, in other words octanoate stabilises larger droplets than heptanoate which in turn stabilises larger droplets than hexanoate, at the same *y* values and polydispersity is higher for octanoate than for the lower two homologues, in line with the observations made in [28], only instead of adding more additive to the composition of ideally mixed microemulsions at a particular *w* value, additive is more present due to stronger adsorption at the interface.

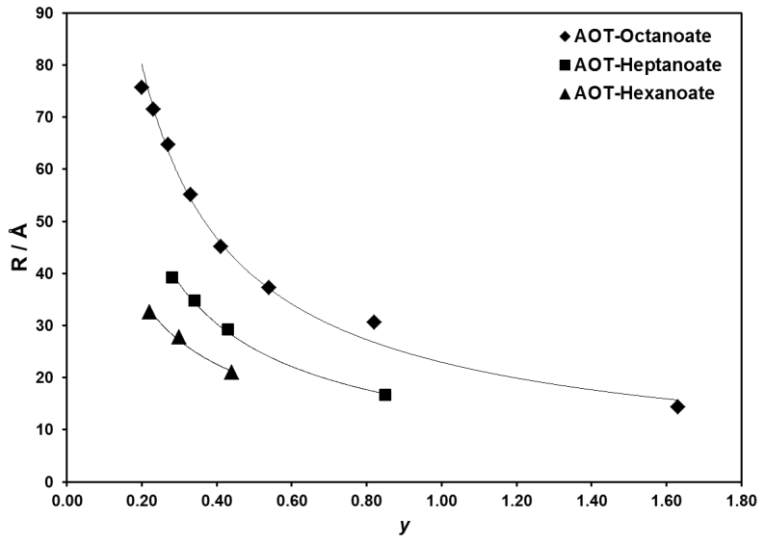

Figure 5. Fitted radii of AOT-alkanoates against *y* which is the ratio of the effective concentration of additive in the droplet in relation to the bulk *cac (y = [hydrotrope]$_{aq}$ / cac).*

Effect of alkanoates on the size of the spherical microemulsions

Looking further into the effect of alkanoates on AOT microemulsions and specifically the spherical microemulsions, AOT only microemulsions increase in size in a linear manner with increasing water content *w*, with the intercept reflecting the length of the AOT anion. Examining the spherical microemulsion cases, mixed microemulsions of AOT with alkanoates also increase in a linear fashion (Figure 6 and Table 5), but with a reduced gradient. This reduced gradient could be accounted for by the increased polydispersity observed with increased additive chain length. Though the differences in gradient appear small they have a significant effect in the estimation of the surfactant head group area at the microemulsion interface.

Table 5. Linear dependences of fitted radii with *w* for spherical microemulsions.

AOT*	$\bar{R} = 1.22w + 9.13$
AOT-hexanoate	$\bar{R} = 1.16w + 9.73$
AOT-heptanoate	$\bar{R} = 0.99w + 9.67$
AOT-octanoate	$\bar{R} = 0.92w + 9.13$

*Data from reference 19

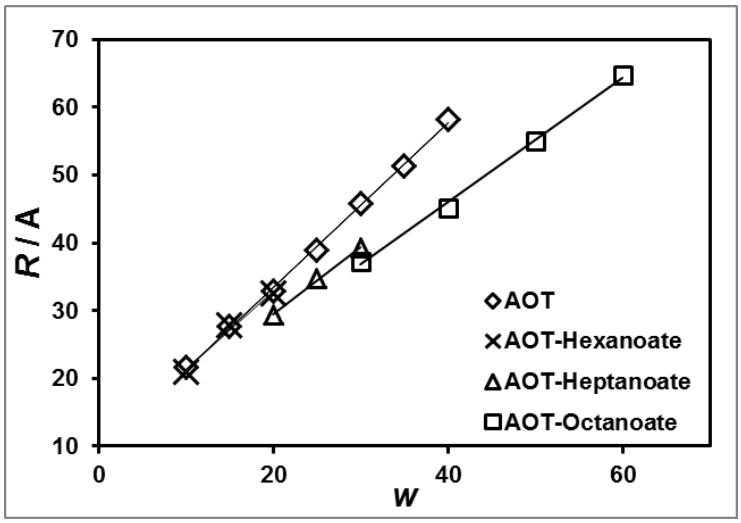

Figure 6. Correlation of fitted radii to *w* for spherical microemulsions.

The slope and intercept of the radii of the equations shown in Table 5 correspond to the gradient and intercept of equation 5 from which the average head group area and volume were determined.

$$\alpha(p)R_c^{av} = \frac{3v_w}{a_h}w + \frac{3v_h}{a_h} \quad 5$$

α(p) is the polydispersity index *(p / R^{av}_c). α(p)* is equal to *1+2p²*. Polydispersity is assumed *w* independent and then α_h is proportional to the gradient, with the intercept being proportional to the head-group volume which is given by combining $\alpha_h=2r_h$ and equation 6.

$$r_h = \left(\frac{3v_h}{4\pi}\right)^{1/3} \quad 6$$

The Porod method for determining radii and head-group areas considers the scattering intensity *I(Q)* reporting from local interface at high *Q* values [19].

$$I(Q)Q^4 = 2\pi\Delta\rho^2\Sigma \quad 7$$

The average area per head group α_h (equation 9) can then be calculated by using equation 7 and equation 8

$$\Sigma = {}^{S}/_{V} \quad 8$$

$$a_h = {}^{\Sigma}/_{N_s} \quad 9$$

S is the total interfacial area and *V* is the unit volume of solution and *Σ* is the total area per unit volume, with all surfactant molecules (N_s) assumed to occupy the interface. An example of a Porod plot is shown in Figure 7.

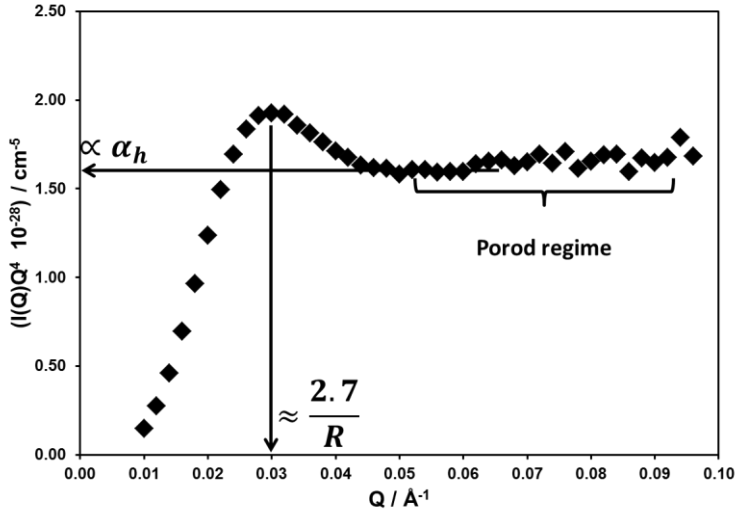

Figure 7. Porod plot of AOT-Octanoate at *w*=60.

The mean head-group areas of the mixed AOT microemulsions are larger than the head-group area for pure AOT microemulsions (Table 6) and between themselves similar, which is also observed for the head-group areas calculated by Porod analysis. As the alkanoates are of the same charge as AOT, the observed increase in average head-group area (α_h) can be attributed to head-group repulsions. This is further substantiated by the calculated head-group radius (r_h) which increases with increasing alkanoate chain length. The intercepts (R_o) reflect a surfactant layer thickness close to that of AOT with all three alkanoates, for which the chain lengths are similar to AOT itself. In Table 7 the chain lengths (l_{max}) of the alkanoates are calculated using the Tanford equation (equation 10) [29]. When averaged with the fitted radius of AOT of 9.1 Å [19] the yielding values ($l_{max\text{-}av}$) are in good agreement to those reported in Table 6, especially considering that the calculated tail length of AOT is 12.57 Å [30].

$$lmax = 1.5 + 1.265n \qquad 10$$

Table 6. Head group areas α_h, volumes v_h and radii r_h deduced from correlation of fitted radii to w for spherical microemulsions, and R_o is the intercept of that linear correlation (Table 5) and corresponds to the length of AOT at the microemulsion interface. The head-group areas were obtained by Porod law analyses.

Composition	$\alpha_h \pm 10$ / Å^2	$v_h \pm 40$/ Å^3	$r_h \pm 0.5$ / Å	$R_o \pm 1$ / Å	α_h *(Porod)* / Å^2
AOT	74.1	225.3	3.77	9.10	69.0*
AOT-Hexanoate	77.6	251.6	3.91	9.73	88.2
AOT-Heptanoate	90.9	292.9	4.12	9.67	84.0
AOT-Octanoate	97.7	297.4	4.14	9.13	82.0

***From reference 19

Table 7. Calculated alkanoate chain lengths l_{max}, average AOT-alkanoate chain lengths $l_{max\text{-}av}$, and observed chain lengths R_o.

n	$l_{max}(= 1.5 + 1.265n)$ / Å	$l_{max\text{-}av}$ / Å	R_o / Å
5	7.83	8.50	9.73
6	9.10	9.10	9.67
7	10.36	9.73	9.13

Conclusions

Hydrotropes are known to promote axial elongation as additives to oppositely charged surfactant systems and generate ellipsoidal or cylindrical nanodroplets in same charge surfactant solutions [8, 9]. Here, alkyl-hydrotropes have been shown to induce strong axial elongation in reverse AOT microemulsions, as additives in the water pools at concentrations in the vicinity and above the corresponding bulk aqueous critical aggregation concentration (*cac* or *cmc*); below this *cac* the droplets become spherical. The hydrotrope chemical structure has an important effect on the microemulsion structure, and it is reasonable to correlate this with the strength of adsorption at the microemulsion interface.

The phase behaviour these mixed AOT reverse microemulsion systems resembles those observed with phenyl-tipped AOT analogues [25] and AOT alkyl-hydrotrope mixtures [18]. In the latter study mixed phase behaviour and solubilisation capacity started resembling that of pure AOT/*n*-heptane/water reverse microemulsions [21] for the longer alkyl chain length hydrotropes. Similarly, here in the case of the alkanoates the solubilization capacity and stability temperature range increase with increasing hydrotrope chain length. For the two hydrotropes a lower stability range and water capacity is observed as in the case of the lower homologues of the alkyl-hydrotropes studied previously [18].

In examining the effects of the additives on the microemulsion geometry the two aforementioned parameters were isolated, by employing short to medium linear alkanoates and small hydrotropes (the parent hydrotropes to the alkyl-hydrotropes studied previously) and studied as a function of additive water content at constant additive to AOT molar ratio. The more hydrophobic sodium benzoate hydrotrope produced axial elongation at the highest effective concentration, however to a lesser extent to the alkylbenzoates reported previously. Sodium cyclohexanoate being more hydrophilic did not exhibit any signs of axial elongation, as the concentrations in the water pool examined were considerably below the *cac*. Interestingly, in the case of the alkanoates axial elongation resulted in ellipsoidal droplets of significant aspect ratio for sodium octanoate and sodium heptanoate at the highest effective water pool concentrations. Sodium hexanoate, like sodium cyclohexanoate, being very hydrophilic and below its *cac* did not induce any structural changes. This is the first report of alkanoates, which have classical surfactant structures, inducing such morphological changes in reverse microemulsions. This leads to the conclusion that the additive molecular structure and strength of adsorption (which can be a function of concentration) are indeed synergistic with the former having the strongest effect. In a previous study [18] the effect of chain length did not appear to directly correlate to the extent of cylinder length.

This study clarifies that molecular architecture, which drives interfacial adsorption, is responsible for the observed phenomenon and emphasises the importance of hydrophobic moiety compatibility of the amphiphiles. Further work should be directed towards ascertaining the absolute amount of additives present in the mixed films

stabilizing these elongated microemulsions, and for this contract variation SANS is the method of choice.

Acknowledgements

MHH thanks Infineum UK and the EPSRC through the University of Bristol School of Chemistry Doctoral Training Account for the provision of a Ph.D. studentship. We also acknowledge ILL, ISIS and STFC for the allocation of beam time, travel and consumables.

References

1. M.A. Lopez-Quintela, C. Tojo, M.C. Blanco, L. Garcıa Rio, J.R. Leis, Current Opinion in Colloid & Interface Science 9 (2004) 264
2. J. Eastoe, M.J. Hollamby, L. Hudson , Adv. Colloid and Interface Sci. 128–130 (2006) 5
3. R. J. de Oliveira, P. Brown, G. B Correia, S. E. Rogers, R. Heenan, I. Grillo, A. Galembeck, J. Eastoe, Langmuir 27 (15) (2011) 9277
4. O. Myakonkaya, B. Deniau, J. Eastoe, S. E. Rogers, A. Ghigo, M. Hollamby, A. Vesperinas, M. Sankar, S. H. Taylor, J. K. Bartley, G. J. Hutchings, ChemSusChem 3 (3) (2010) 339
5. M.F. Nazar, S.S. Shah, M.A. Khosa, Petroleum Science and Technology 29 13 (2011) 1353
6. M.J. Lawrence, G. D. Rees, Adv. Drug Delivery Rev. 45 (2000) 1 89
7. L.K. Hudson, J. Eastoe, P.J. Dowding, Adv. Coll. and Interf. Sci. 123-126 (2006) 425
8. C. A. Dreiss, Soft Matter, 3 (2007) 956
9. Z. Chu, C. A. Dreiss Y. Feng Chem Soc Rev DOI: 10.1039/c3cs35490c
10. L. Ziserman, L. Abezgauz, O. Ramon, S.R. Raghavan, D. Danino, Langmuir 25 (2009) 10483
11. A. R. Rakitin and G. R. Pack Langmuir 21 (2005) 837
12. V. G. Gaikar, K. V. Padalkar, and V. K. Aswal, J. Mol. Liq. 138(1-3) (2008) 155
13. C. Petit, P. Lixon, M.P. Pileni, Langmuir 7 (1991) 2620
14. J. Eastoe, F. Giovanna, B.H. Robinson, T. Towey, R.K. Heenan, F. Leng, J. Chem. Soc. Faraday Trans. 88 (1992) 461
15. J. Eastoe, T.F. Towey, B. Robinson, J. Williams, R.K. Heenan, J. Phys. Chem. 97, (1993) 1459
16. J. Eastoe, D.C. Steytler, B. Robinson, R.K. Heenan, A.N. North, J.C. Dore, J. Chem. Soc. Faraday Trans. 90 (1994) 2479
17. K. Trickett, D. Xing, R. Enick, J. Eastoe, M.J. Hollamby, K.J. Mutch, S.E. Rogers, R.K. Heenan, D.C. Steytler, Langmuir 26 (2010) 83
18. M. Hopkins Hatzopoulos, J. Eastoe, P.J. Dowding, I. Grillo J. Colloid Interface Sci. 392 (2013) 304

19. S. Nave, J. Eastoe, R.K. Heenan, D.C. Steytler, Langmuir 16 (2000) 8741
20. M. Hopkins Hatzopoulos, J. Eastoe, P. J. Dowding, S.E. Rogers, R. Heenan, R. Dyer Langmuir 27 (2011) 12346
21. R. K. Heenan, The “FISH” Data Fitting Program Manual; Rutherford Appleton Laboratory Report RAL-89-129
22. Klevens, H. B. J. Phys. Colloid Chem. 52 (1948) 130
23. M. Hopkins Hatzopoulos, J. Eastoe, P.J. Dowding, I. Grillo, B. Demé, S.E. Rogers, R. Heenan, R. Dyer Langmuir 28 (2012) 9332
24. A.N. Campbell, G.R. Lakshminarayanan, Canadian Journal of Chemistry 43 (1965) 1729
25. S. Nave, A. Paul, J. Eastoe, A.R. Pitt, R.K. Heenan, Langmuir 21 (2005) 10021
26. J. Eastoe, Surfactant Chemistry, Wuhan University Press (2005)
27. A. Bumajdad, J. Eastoe, R.K.Heenan, Langmuir 19 (2003) 7219
28. J.Eastoe, A.Bumajdad, R.K.Heenan, J.R.Lu, D.C.Steytler and S.Egelhaaf, J. Chem. Soc. Faraday Transactions 94 (1998) 2143
29. C. Tanford, The Hydrophobic Effect, 2nd ed.; Wiley: New York, 1980
30. E. Y. Sheu, S.-H. Chen, J.S. Huang J. Phys. Chem. 91 (1987) 3306